Polymer 51 (2010) 6151–6160

Contents lists available at ScienceDirect

Polymer

journal homepage: www.elsevier.com/locate/polymer

# Cationic photopolymerization of epoxides containing carbon black nanoparticles

Cindy C. Hoppe [a], Beth A. Ficek [b], Ho Seop Eom [a], Alec B. Scranton [a,*]

[a] Department of Chemical and Biochemical Engineering, The University of Iowa, 4133 Seamans Center, Iowa City, IA 52242, USA
[b] DSM Desotech, Inc., 1122 St. Charles Street, Elgin, IL 60120, USA

ARTICLE INFO

*Article history:*
Received 13 August 2010
Received in revised form
28 October 2010
Accepted 29 October 2010
Available online 4 November 2010

*Keywords:*
Cationic photopolymerization
Carbon black
Nanocomposites

ABSTRACT

The active centers responsible for cationic photopolymerizations are essentially non-terminating, and continue to propagate after the illumination is ceased. In this contribution, the mobility of the long-lived cationic active centers is investigated for the cure of epoxides containing carbon black nanoparticles. Concentration profiles for the cationic active centers produced during illumination were coupled with an analysis of the active center reactive diffusion during the post-illumination period, revealing that migration of the active centers leads to cure beyond the illuminated depth. A kinetic analysis yielded predicted cure times for coatings of varying thickness and carbon black loading, showing good agreement with experimental results obtained for photopolymerizations of cycloaliphatic diepoxide coatings containing a monodisperse carbon black with mean hydrodynamic radius of 29.2 nm. These results indicate that the long lifetimes and reactive diffusion of cationic active centers may be used for effective curing of coatings containing carbon black nanoparticles. This comprehensive approach could be applied to other opaque nanocomposite systems.



## 1. Introduction

Photopolymerization is well established as an effective method for curing transparent films and coatings. However, photopolymerization reactions are hindered by the presence of particles and fillers which directly compete with the photoinitiator by absorbing the incident radiation [1]. This results in increased light attenuation in coatings and films containing nanoparticles or pigments. Nanoparticles are commonly used to improve the abrasion resistance and toughness of polymers; however these materials generally must be thermally cured [2–5]. The spatial and temporal control of the initiation reaction afforded by the use of light, rather than heat, to drive the polymerization offers a number of important process advantages. For this reason, a number of investigators have pursued methods for effectively photocuring acrylates or epoxides containing nanoparticles. For example, many investigators have reported the photopolymerization of nanocomposites containing iron oxide nanoparticles [6], functionalized organoclays [7], and functionalized silica [8,9]. Sangermano and collaborators found that the presence of the functionalized organoclays had little effect on the photopolymerization kinetics [7], and Chemtob et al. reported that the high UV-transmittance of nanosilica fillers ensures photopolymerization of the monomer while maintaining optical transparency in the cured film [9]. Sangermano and collaborators [10,11] recently reported hybrid photopolymerization/sol–gel reaction processes to produce coatings containing nano-scale inorganic domains. In this clever approach, the inorganic domains are produced *in situ*, after the UV curing step, and the investigators demonstrated that coatings with desirable scratch resistance, toughness, clarity, and refractive index could be obtained.

In the photopolymerized nanocomposites discussed above, the presence of the nanoparticle does not prevent light penetration either because the system is transparent, or the thickness of the coating is not large enough to cause significant light attenuation. In contrast, this contribution examines photopolymerizations of systems in which the presence of the nanoparticle prevents sufficient light penetration to the desired depth of polymerization. Specifically, cationic photopolymerizations of epoxide systems containing carbon black nanoparticles are investigated. Cationic polymerizations are attractive for this purpose due to the long lifetime and mobility of the cationic active centers. Unlike free radicals, cationic active centers are not inhibited by oxygen and are essentially non-terminating, and therefore have been shown to remain active long after irradiation has ceased and may lead to further polymerization in the illuminated region (dark cure). Dark cure in cationic photopolymerizations of epoxide monomers has been characterized by a number of investigators [12–14]. In addition, cationic active centers may lead to “shadow cure” in unexposed depths and regions shaded by opaque constituents or fillers.

* Corresponding author. Tel.: +1 319 335 1414; fax: +1 319 335 1415.
*E-mail address:* alec-scranton@uiowa.edu (A.B. Scranton).

0032-3861/$ – see front matter © 2010 Elsevier Ltd. All rights reserved.
doi:10.1016/j.polymer.2010.10.057

For example, in a recent contribution, Ficek et al. [15] characterized the diffusion of the cationic active centers in photopolymerizations of cycloaliphatic epoxides, and demonstrated that the cure can continue for several hours to extend deep below the illuminated surface in unfilled systems.

This contribution provides a theoretical and experimental investigation of cationic photopolymerizations of epoxide coatings containing carbon black nanoparticles. The fundamental differential equations describing the polychromatic photoinitiation process [16,17] are solved to obtain profiles of the concentration of active centers as a function of time and depth. Here the differential reaction/diffusion equations which describe the consumption of photoinitiator and production of active centers are coupled to the differential absorption equation which accounts for the polychromatic absorption by all system components, including the carbon black. During the illumination period the active centers are preferentially generated at the surface to produce a concentration gradient that leads to diffusion into the regions of unexposed monomer. Using the active center concentration gradient at the end of the illumination period as the initial condition for the differential diffusion equation allows the active center concentration profile to be determined long after the illumination has ceased. Coupling these concentration profiles with the propagation rate equation for low to intermediate conversions allows the cure time, or time for macroscopic property development, to be predicted for a required conversion. In this manner, experimental cure times for cationically polymerized epoxide coatings containing carbon black are compared with theoretical predictions of cure time.

## 2. Experimental

### 2.1. Materials

The cationically polymerizable monomer 3,4-epoxy-cyclohexylmethanyl 3,4-epoxy-cyclohexanecarboxylate (EEC, Sigma Aldrich) was used in these experiments. The photoinitiator used in these experiments was (tolycumyl)iodonium tetrakis (pentafluorophenyl) borate (IPB, Secant Chemicals). The carbon black studied was CB-35 (NIPex 35, Degussa Engineered Carbons, LP). Methanol and propylene carbonate solvents were used for UV/Visible spectroscopy.

### 2.2. Carbon black dispersion and size characterization

The carbon black used in this study is a commercial furnace black designed for chemically prepared toner applications because of its ease of dispersion. Furnace blacks generally exhibit a hydrophobic, non-polar, basic character. Propylene carbonate was selected as a solvent for carbon black spectral measurements because it is a polar aprotic solvent in which the nanoparticles exhibit good dispersion. The size and monodispersity of CB-35 carbon black in propylene carbonate was characterized using dynamic light scattering (DLS). Experiments were carried out with a DynaPro 99P instrument (Protein Solutions) equipped with a 1 cm pathlength cell. Samples were analyzed using the Dynamics software provided with the instrument. The DLS results showed the sample to exhibit a monodisperse and unimodal distribution of particle sizes with a mean hydrodynamic radius of 29.2 nm.

### 2.3. UV/Visible spectroscopy

The absorbance spectra for the monomer, photoinitiator, photolysis products, and carbon black were determined in 1 nm increments using an 8453 UV–Visible spectrophotometer (Agilent Technologies). For the monomer and photoinitiator, the spectra were obtained for dilute solutions ($10^{-2}$ M and $10^{-3}$ M respectively) in propylene carbonate (a non-polymerizable solvent which approximates the monomer) placed in an air-tight, quartz cell to prevent any changes in concentration due to evaporation of the solvent. To obtain the absorbance spectra after photolysis, the photoinitiator samples were illuminated with a 200 Watt Hg–Xe arc lamp (Oriel Light Sources) until there was no change in the absorbance spectrum. For carbon black spectra, the nanoparticles were dispersed in propylene carbonate (~1 g/L) by mixing on a stir plate for at least 24 h prior to analysis.

### 2.4. Raman spectroscopy for characterization of the propagation rate constant

The propagation rate constant for cationic polymerization of the cycloaliphatic diepoxide used in this study was determined independently for the neat monomer using Raman Spectroscopy. Raman spectra were collected using a holographic fiber-coupled stretch probehead (Mark II, Kaiser Optical Systems, Inc.) attached to a modular research Raman spectrograph (HoloLab 5000R, Kaiser Optical Systems, Inc). A sample containing EEC monomer with photoinitiator was placed inside a sealed 1 mm ID quartz capillary tube. A 200 mW 785 nm near-infrared laser through a 10× non-contact sampling objective with 0.8 cm working distance was directed into the sample to induce the Raman scattering effect. Photopolymerization was initiated by simultaneously illuminating the sample with a 100 W high pressure mercury lamp (Acticure Ultraviolet/Visible Spot Cure System, EXFO Photonic Solutions, Inc.). The output of the lamp was filtered for 250–450 nm wavelengths, resulting in an overall irradiance of 100 mW/cm$^2$ in this range. The Raman peak at 790 cm$^{-1}$ was used to determine the epoxide conversion [18]. The effective propagation rate constant, $k_p$, was determined using a previously published procedure [19].

### 2.5. Photopolymerization of coatings

The time required for the coatings containing CB-35 to reach a tack-free cure was investigated over a range of loadings and illumination times. For these experiments, solutions containing 96–99 wt% EEC, 1 wt% IPB, and 0–3 wt% carbon black were mixed together for 24 h in dark conditions. The solutions were then spread onto aluminum substrates using a draw bar to achieve the desired uniform coating thickness (40 or 80 μm). The coated panels were then illuminated for various times, using a 200 W Hg–Xe arc lamp. The output of the lamp was passed through a water filter to eliminate infrared light, resulting in an overall irradiance of 50.0 mW/cm$^2$. The wavelength range of interest was determined to be 295–307 nm, corresponding to the overlap between the photoinitiator absorbance spectrum and the lamp emission spectrum. The irradiance in this range was determined to be 5 mW/cm$^2$, measured using a calibrated miniature fiber optic spectrometer (USB4000, Ocean Optics, Inc.). The photopolymerization was carried out under atmospheric conditions and at room temperature. After exposure, the panels were stored at room temperature. The cure time required for macroscopic property development was determined by characterizing the surface tack and the adhesion to the substrate at regular intervals. Once full property development was achieved, the thickness of the coating was obtained by a micrometer (micro-TRI-gloss μ, BYK Gardner).

## 3. Results and discussion

### 3.1. Photoinitiator, photolysis product, and carbon black absorptivities

A number of investigators have shown that free-radical photoinitiators typically exhibit significant photobleaching [21–23] since

the absorption of the photolysis products is lower than that of the original photoinitiator. Photobleaching is important for photocuring of thick systems since it allows light to penetrate deeper beneath the illuminated surface upon production of active centers [24–28]. Photobleaching during cationic photopolymerizations has received considerably less attention in the literature, and the degree of photobleaching of most cationic photoinitiators has not been characterized. Table 1 shows the molar absorptivity as a function of the incident wavelength (for the wavelengths of interest in this study) for the both the original cationic photoinitiator (IPB) and the photolysis products. This table illustrates that, although the IPB photoinitiator exhibits some photobleaching upon photolysis, the molar absorptivity of the photolysis products is significant (average 34% of the photoinitiator absorptivity).

The optical properties of the nanoparticle fillers play an important role for the potential photopolymerization of nanocomposite coatings. In general, nanoparticles or pigments may reduce light penetration by absorption, scattering or reflection of the incoming light, therefore the radiative flux in a nanoparticle filled system can be characterized by accounting for these effects. This has been accomplished for highly reflective additives, such as titanium dioxide, by describing the specular and diffuse reflectance using a four-flux model [29]. In one study of Pigment Red 254, Jahn and Jung [30] found the reflectance contribution to be negligible for particles smaller than 100 nm. Similarly, for a matrix containing carbon black, Tesfamichael et al. [31] found that the contribution of the reflectance was insignificant for incident wavelengths below 500 nm. The system under investigation meets both of these criteria since the mean particle hydrodynamic radius is less than 30 nm and the initiating light falls in a narrow wavelength region where the UV photoinitiator absorption overlaps with the 200 W Hg–Xe arc lamp emission (295–308 nm). These observations suggest that the reflectance and scattering effects can be neglected for the small, monodisperse carbon black particles used in this study. This assumption was further confirmed by measuring the absorbance of the carbon black at different positions between the emission beam window of the UV/Visible spectrophotometer and the detector window. Spectra were collected at three different positions within this window, 6 cm increments over a range of 12 cm. The spectra at all positions were identical, confirming that the reflectance/scattering contributions can be neglected for this particular system. To confirm that the absorption is linearly dependent upon the CB-35 loading, the direct transmittance in the wavelength range of interest (295–308 nm) was measured as a function of carbon black mass concentration. The linear correlation coefficient for a plot of the absorbance as a function of concentration was 0.9999, with an effective absorptivity of 22.9 L/g-cm, which remains constant over the incident wavelength range. This value for the absorptivity of CB-35 was used throughout the remainder of this paper.

**Table 1**
Napierian molar absorptivities (L/mol-cm) for photoinitiator ($\varepsilon_i$) and photolysis products ($\varepsilon_p$) for incident wavelengths.

| $\lambda$ (nm) | $\varepsilon_i$ | $\varepsilon_p$ | $\varepsilon_p/\varepsilon_i$ |
|---|---|---|---|
| 295 | 2736 | 1046 | 0.38 |
| 296 | 2537 | 936 | 0.37 |
| 297 | 2352 | 839 | 0.36 |
| 298 | 2175 | 753 | 0.35 |
| 299 | 2005 | 677 | 0.34 |
| 300 | 1844 | 610 | 0.33 |
| 301 | 1688 | 549 | 0.33 |
| 302 | 1544 | 496 | 0.32 |
| 303 | 1409 | 450 | 0.32 |
| 304 | 1282 | 410 | 0.32 |
| 305 | 1164 | 373 | 0.32 |
| 306 | 1054 | 342 | 0.32 |
| 307 | 954 | 315 | 0.33 |

### 3.2. Determination of the active center concentration profiles produced during illumination

An accurate description of the spatial photoinitiation profiles produced during the illumination step is necessary to predict the depth of cure in a nanoparticle filled system. The evolution of the light intensity gradient and the corresponding active center concentration profiles were found using the following set of differential equations for polychromatic illumination, including diffusion of the initiator and photolysis products:

$$\frac{\partial C_i(z,t)}{\partial t} = -\frac{C_i(z,t)}{N_A h}\sum_j\left(\frac{\varepsilon_{ij}\phi_j I_j(z,t)}{\nu_j}\right) + D_i\frac{\partial^2 C_i(z,t)}{\partial z^2} \tag{1}$$

$$\frac{\partial C_p(z,t)}{\partial t} = \frac{C_i(z,t)}{N_A h}\sum_j\left(\frac{\varepsilon_{ij}\phi_j I_j(z,t)}{\nu_j}\right) \tag{2}$$

$$\frac{\partial I_j(z,t)}{\partial z} = -\left[\varepsilon_{ij}C_i(z,t) + \varepsilon_{pj}C_p(z,t) + a_{CBj}C_{CB} + A_m\right]I_j \tag{3}$$

Here, $z$ is the direction perpendicular to the illuminated surface, with $z=0$ at the illuminated edge. The subscript $j$ is an index with a different value for each wavelength of light under consideration; $C_i(z,t)$ is the initiator molar concentration at depth $z$ and time $t$; $C_p(z,t)$ is the photolysis product molar concentration at depth $z$ and time $t$; $I(z,t)$ is the incident light intensity of a specific wavelength at depth $z$ and time $t$ with units of mW/cm$^2$; $\varepsilon_i$ is the initiator Napierian molar absorptivity at a specific wavelength with units of L/mole-cm; $\varepsilon_p$ is the photolysis product Napierian molar absorptivity at a specific wavelength with units of L/mole-cm; $a_{CB}$ is the carbon black Napierian absorptivity at a specific wavelength with units of L/g-cm; $C_{CB}$ is the carbon black mass concentration in units of g/L; $\varphi_i$ is the quantum yield of the initiator at a specific wavelength, defined as the fraction of absorbed photons that lead to fragmentation of the initiator; $N_A$ is Avogadro's number; $h$ is Plank's constant; $\nu$ is the frequency of light in units of inverse seconds; $D_i$ is the diffusion coefficient of the initiator in units of cm$^2$/sec; and $A_m$ is the absorption coefficient of the monomer and the polymer repeat unit with units of 1/cm. Note that the Napierian absorptivities are used because they are most natural for the differential version of the absorption equation (Equation (3)). The quantum yield for IPB is 0.7 and the diffusion coefficients are $1\times10^{-7}$ cm$^2$/s [32].

For a polymerization system of thickness $z_{max}$ which is illuminated at the planar surface in which $z=0$, the following initial and boundary conditions apply [16,17]:

$$C_i(z,0) = C_o \tag{4}$$

$$C_p(z,0) = 0 \tag{5}$$

$$\frac{\partial C_{i,p}}{\partial z} = 0 \text{ at } z = 0 \text{ and } z = z_{max} \tag{6}$$

$$I(0,t) = I_o \tag{7}$$

Equation (4) states that the initial initiator concentration, $C_o$, is uniform throughout the depth of the sample. Similarly, Equation (5) indicates that the initial photolysis product concentration is zero throughout the sample. Equation (6), the no-flux boundary condition,

indicates that there is no transport of initiator or photolysis product across the illuminated surface or the opposite boundary (typically an interface with a substrate). Finally, Equation (7) states that the light intensity on the illuminated surface is constant and equal to the initial intensity, $I_o$.

*3.2.1. Active center profiles for infinitely thick systems*

To demonstrate the effect of the carbon black nanoparticles on the photoinitiation process, it is useful to examine simulation results for an infinitely thick system where $z_{max} = \infty$. Simultaneous solution of Equations (1)–(7) yields profiles of light intensity and initiator concentration as functions of depth at various instants in time for an infinitely thick system. Fig. 1 contains plots of the light intensity as a function of depth for two different EEC systems: one unfilled (Fig. 1A) and the other containing 3 wt% CB-35 (Fig. 1B). The figure illustrates that the presence of the carbon black has a marked effect on the initial light intensity gradient in the sample. In the system containing carbon black, the light intensity drops to a value of essentially zero in less than 60 μm. In contrast, for the unfilled case the initial light intensity is still 75% of the incident value at a depth of 60 μm, and retains more than 10% at a depth of 500 μm. The photobleaching described in Table 1 leads to the change in the gradient with increasing illumination time for the unfilled system (Fig. 1A), and is negligible for the system containing carbon black (Fig. 1B) due to the strong absorption by the nanoparticles.

Since the rate of consumption of the photoinitiator at a given depth increases with increasing total light intensity (as described in Equation (1)), the initial rate is highest at the illuminated surface, and is zero anywhere in which the total light intensity is zero. Therefore, a photoinitiator concentration gradient will be established immediately upon illumination, and will evolve with time in a manner described by the simultaneous solution of Equations (1)–(7). For example, Fig. 2 shows profiles of the photoinitiator concentration as a function of depth with increasing illumination time for the cationic photopolymer system with and without 3 wt% CB-35. These results illustrate that in the system containing carbon black (Fig. 2B), the photoinitiator is depleted rapidly at the surface of the sample where the light intensity is highest, but the photoinitiation reaction does not extend much beneath the surface due to the light attenuation caused by the strongly absorbing carbon black nanoparticles. As a result, the system containing CB-35 exhibits sharp gradients in both the light intensity (Fig. 1B) and the initiator concentration (Fig. 2B). Compared to the unfilled system (Fig. 2A), this steep concentration gradient results in a stronger driving force for diffusion of the photoinitiator, therefore the diffusive contributions during illumination are much more important for the system containing carbon black. Diffusion of the photoinitiator during the illumination period is responsible for the concentration change that takes place at depths where the light intensity is zero (depths greater than 60 μm). The local rate of active center generation is equal to the product of the local initiator concentration and the local light intensity summed over the initiating wavelengths [16,17].Since the cationic active centers are essentially non-terminating, and each photoinitiator molecule leads to the formation of a single active center molecule, the cationic active center concentration, $C_{AC}$, at a given depth, $z$, and time, $t$, can be determined from the integrated form of the rate equation:

$$C_{AC}(z,t) = \int_0^t C_i(z,t) \sum_j [I(z,t)]_j \phi_j \varepsilon_{ij} \mathrm{d}t \tag{8}$$

Fig. 3 shows the evolution of the active center concentration profiles during the 5 min illumination time for two different loadings. The 3 wt% CB-35 system in Fig. 3B shows the active center concentration profiles within the first 300 μm of an infinitely thick system, resulting from the light intensity shown in Fig. 1B and the photoinitiator concentration shown in Fig. 2B. These results are compared with the active center concentration profiles for a 2 wt% CB-35 system shown in Fig. 3A. The concentration of active centers generated at the illuminated surface of the sample is slightly higher for the 2 wt% system. The concentration drops off quickly to a value of zero within the first ~200 μm of sample depth for the 3 wt% CB-35 system. Diffusion of the propagating active centers during the illumination period are neglected, since the illumination period for these systems are very short compared with the post-illumination periods studied in the remainder of this contribution.

*3.2.2. Active center profiles for coatings containing carbon black*

For coatings of a finite thickness, the active center concentration profiles predicted during the illumination period differ from those for an infinitely thick system due to the no-flux boundary condition at the interface between the coating and the substrate. Fig. 4 shows the active center concentration profiles throughout the depth of an 80 μm thick coating during 5 min of illumination for 2 wt% CB-35

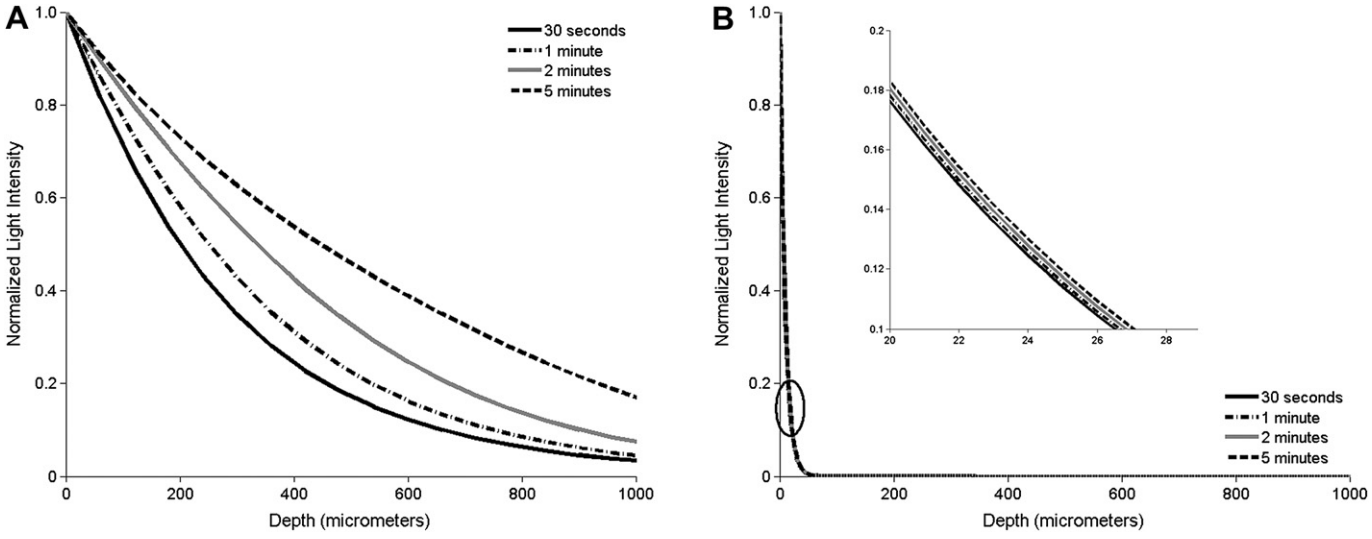


**Fig. 1.** Profiles of the initial total light intensity summed over initiating wavelengths (295–308 nm). A) no pigment, B) 3 wt% CB-35. Monomer: EEC, Initiator: 1 wt% IPB.

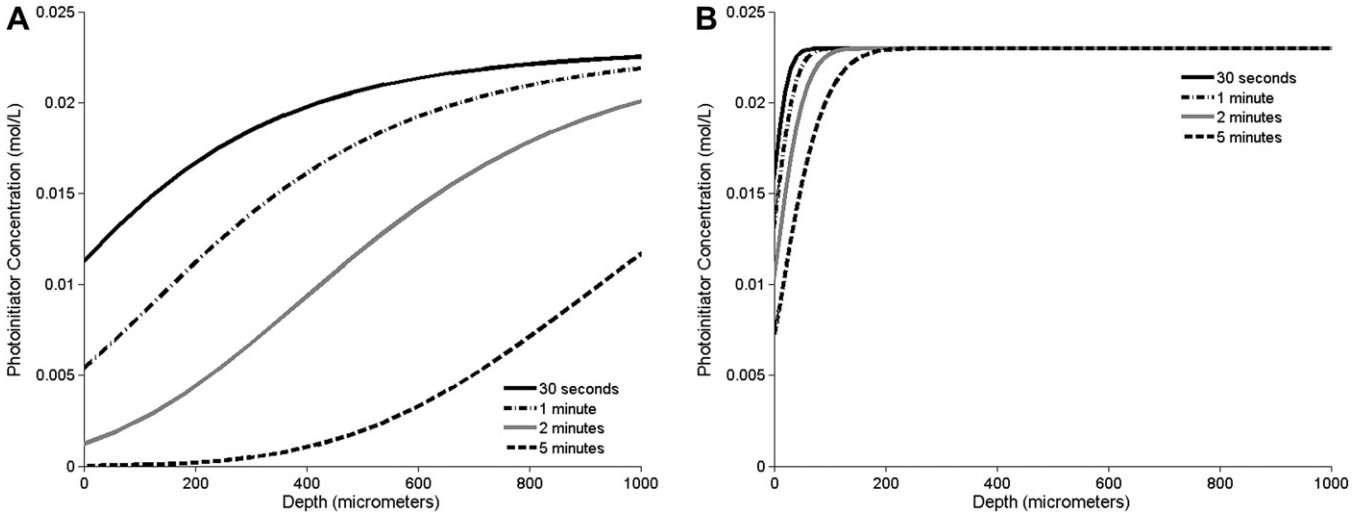


**Fig. 2.** Profiles of photoinitiator concentration after 2 min illumination. A) no pigment, B) 3 wt% CB-35. Monomer: EEC, Initiator: 1 wt% IPB.

(Fig. 4A) and 3 wt% CB-35 (Fig. 4B). In contrast to the infinitely thick case (Fig. 3), the concentration gradients for the 80 μm coatings are not as steep at a given illumination time. This arises from the fact that the diffusion of the active centers is confined to the finite thickness of the coating, therefore the concentration at the interface increases more rapidly with time. For example, the active center concentration at the bottom of the 80 μm thick 2 wt% CB-35 coating after 5 min of illumination is 0.012 mol/L (from Fig. 4A), whereas the value at the position of 80 μm depth in the infinitely thick system (Fig. 3A) is 0.005 mol/L. The comparison between Fig. 4A and B reveals the effect of the carbon black loading on the active center concentration profiles. An increased loading decreases the active center concentration at a given location and time, due to the effect of the carbon black on the light intensity gradient.

The effect of the interface no-flux boundary condition on resulting active center profile becomes more pronounced as the coating thickness is reduced, as illustrated in Fig. 5. Fig. 5A and b show the active center concentration profiles at specific illumination times (2 min and 5 min respectively) for coating thicknesses ranging from 40 μm to infinitely thick, for 2 wt% CB-35. The figure illustrates that the active center concentration profiles for the infinitely thick systems decrease relatively sharply and reach a value of zero concentration at a depth of 140 μm for a 2 min illumination time and 220 μm for an illumination time of 5 min. The profiles for the infinitely thick case provide an asymptotic limit for the coatings of finite thickness. Specifically, the active center concentration profiles approach those of the infinitely thick case as the coating thickness is increased or the illumination time is decreased. The figure also illustrates that the active center concentration profile becomes more uniform throughout the thickness of the coating as the thickness is decreased or the illumination time is increased. These trends arise from the fact that the diffusion of the active centers is confined to the finite thickness of the coating. In the case of the 40 μm thick coating, the concentration is nearly uniform throughout the thickness of the coating after 5 min of illumination.

### 3.3. Post-illumination diffusion of active centers in coatings containing carbon black

During the illumination period, active center profiles decrease sharply with depth, resulting in a concentration gradient and

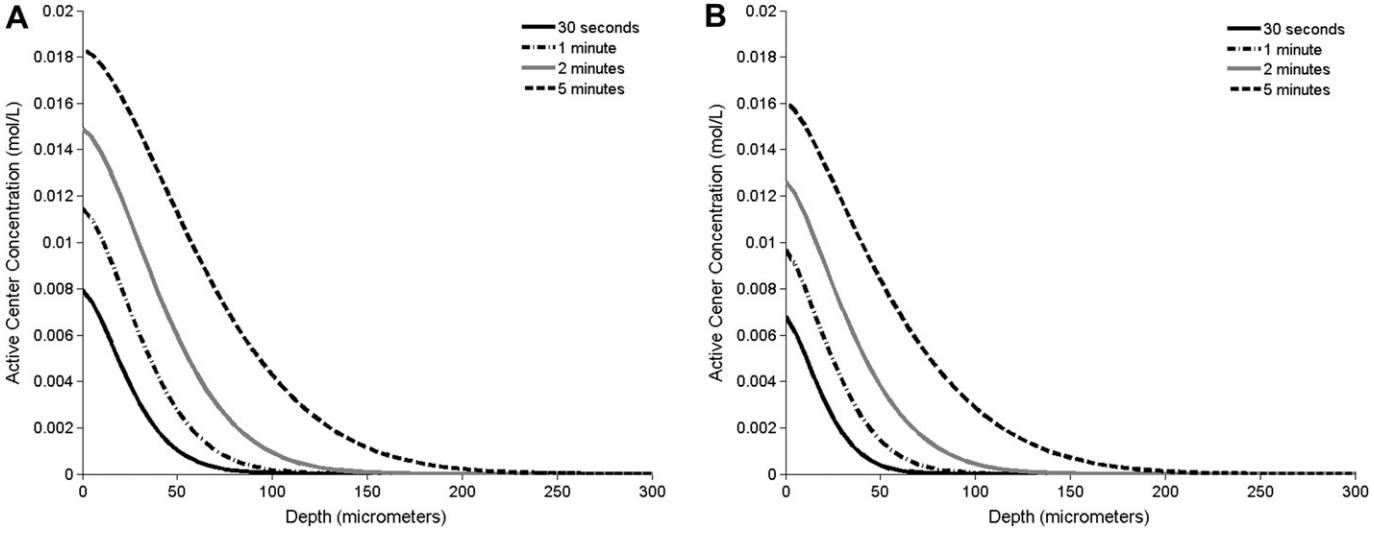


**Fig. 3.** Profiles of active center concentration for infinite thickness during 5 min of illumination. A) 2 wt% CB-35, B) 3 wt% CB-35. Monomer: EEC, Initiator: 1 wt% IPB.

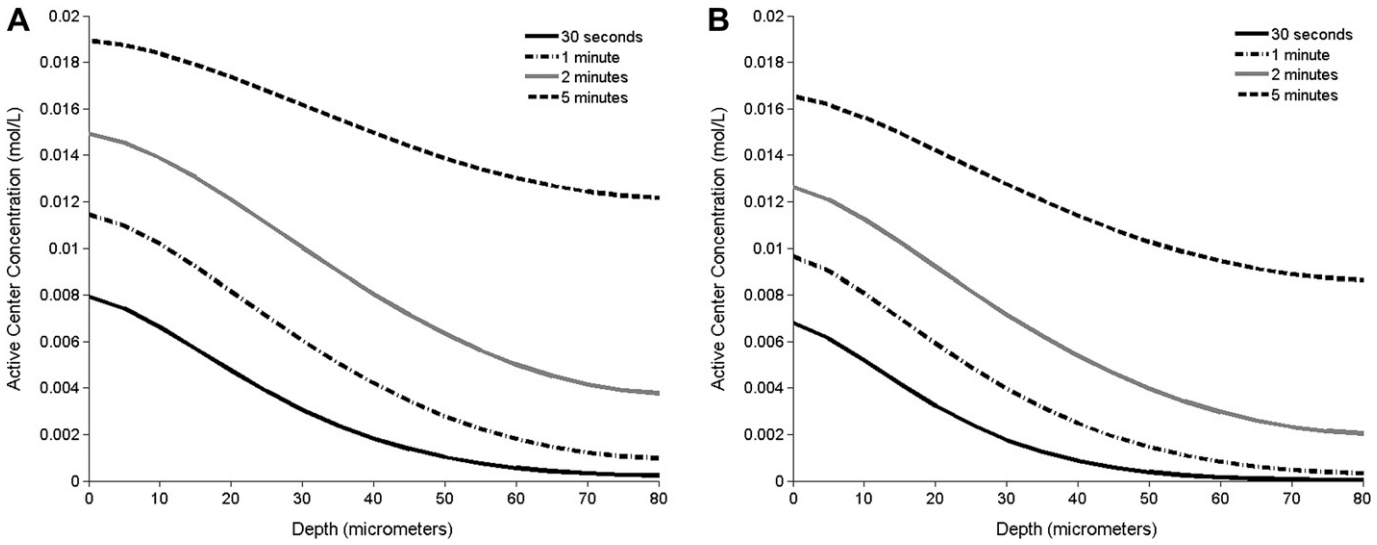


**Fig. 4.** Profiles of active center concentration for 80 μm thick coatings during 5 min of illumination. A) 2 wt% CB-35, B) 3 wt% CB-35. Monomer: EEC, Initiator: 1 wt% IPB.

therefore a driving force for diffusion. Diffusion of the active centers during the post-illumination period is described by Fick's Second Law

$$\frac{\partial C_{AC}(z,t)}{\partial t} = D_{AC}\frac{\partial^2 C_{AC}(z,t)}{\partial z^2} \tag{9}$$

where $C_{AC}$ corresponds to the concentration of active centers, and $D_{AC}$ is the diffusion coefficient of active centers in $cm^2$/sec. The initial condition for the active center concentration as a function of depth is the profile obtained by applying Equation (8) at the end of the illumination period for each desired depth increment. In addition, the no-flux boundary condition indicates that there is no transport of initiator or photolysis product across the illuminated surface ($z = 0$) or the substrate boundary ($z = z_{max}$).

$$\frac{\partial C_{ac}(t,z)}{\partial z} = 0 \text{ at } z = 0 \text{ and } z = z_{max} \tag{10}$$

The diffusion coefficient for active centers generated by the IPB photoinitiator in the cycloaliphatic diepoxide containing 1 wt% carbon black was determined using a previously described experimental protocol [15], and was determined to be $1 \times 10^{-7}$ $cm^2$/s, which is a reasonable value for reactive diffusion in which the active centers migrate by propagating with unreacted monomers. Reactive diffusion has been identified as the primary mode for active center mobility in free-radical polymerizations of multifunctional acrylates [33] and cationic polymerizations of divinyl ethers [19,34].

Numerical solution of Equations (9) and (10) yields profiles of the active center concentration diffusing with increasing post-illumination time into a coating of finite thickness. Fig. 6A and B show the active center profiles for an 80 μm coating containing 2 wt % and 3 wt% CB-35, respectively, with increasing post-illumination time. As shown in Fig. 4, the active center concentration profile exhibits a gradient at the end of the illumination period. Fig. 6 indicates that the active center concentration becomes uniform throughout the thickness of the 80 μm coating within 10 min post-illumination due to diffusion of the active centers. The comparison between Fig. 6A and B illustrates that the final uniform active center concentration increases as the carbon black loading is

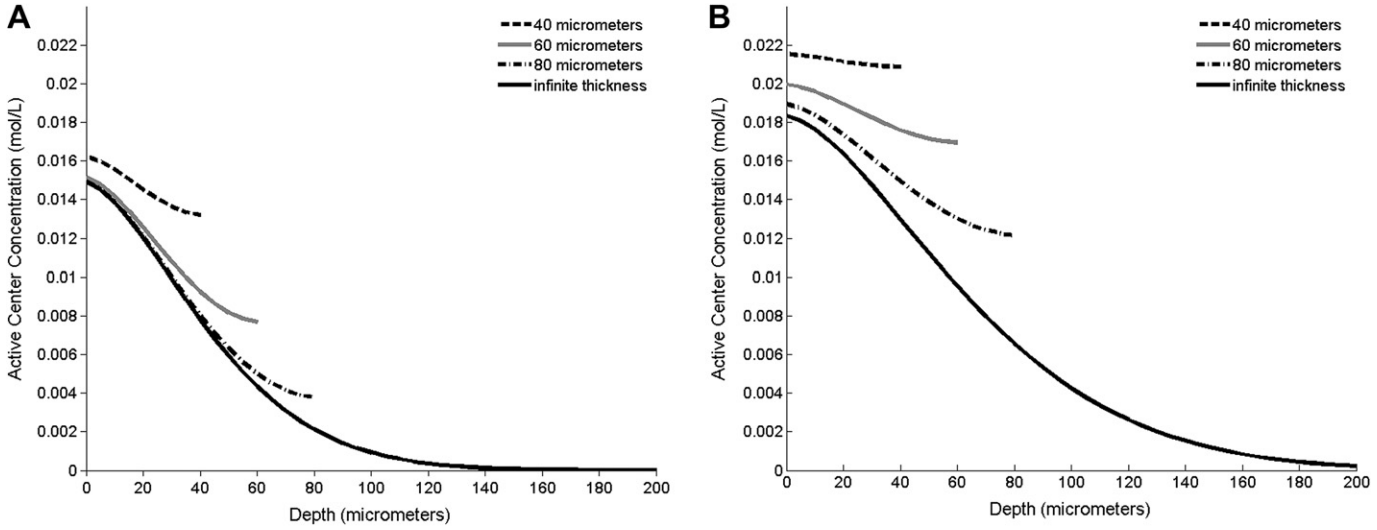


**Fig. 5.** Profiles of active center concentration for 2 wt% CB-35 pigmented coatings ranging from 40 μm to infinitely thick. A) 2 min of illumination, B) 5 min of illumination. Monomer: EEC, Initiator: 1 wt% IPB.

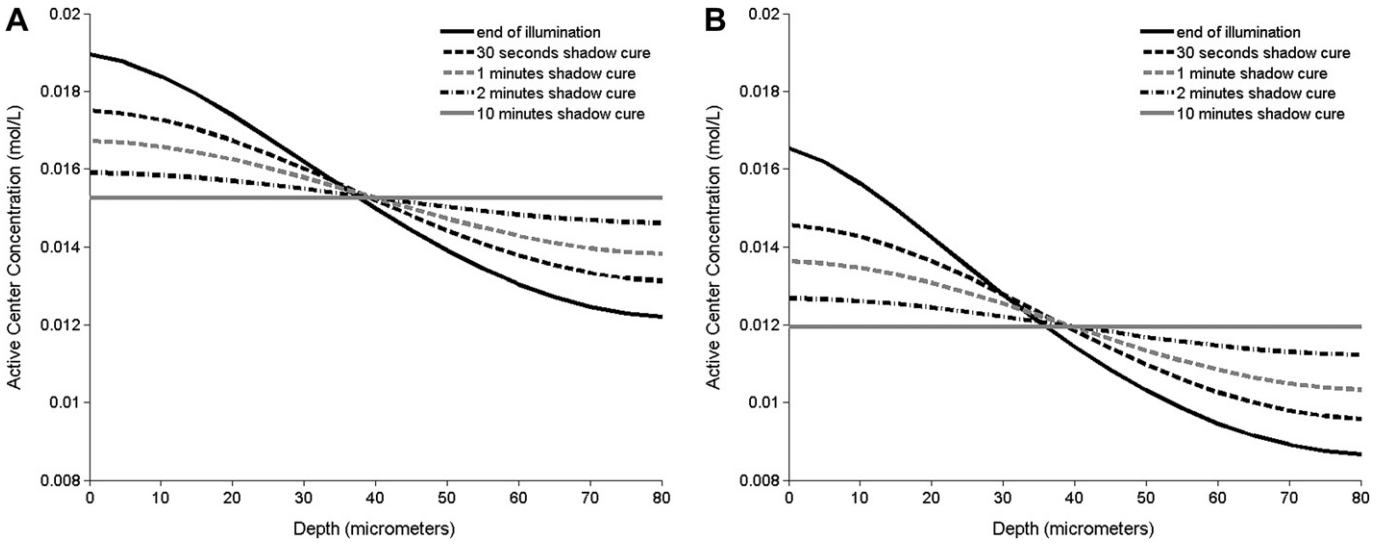


**Fig. 6.** Active center concentration profiles diffusing post-illumination in pigmented coating (80 μm thick). A) 2 wt% CB-35, B) 3 wt% CB-35. Monomer: EEC, Initiator: 1 wt% IPB, Exposure time: 5 min.

decreased since a higher fraction of the photoinitiator undergoes photolysis as the competitive absorption by the CB-35 is decreased.

Shorter illumination times were used to demonstrate the post-illumination diffusion of active centers in a 40 μm thick coating containing carbon black. According to the results shown in Fig. 5, the active center concentration profile was nearly uniform throughout the thickness of the coating after 5 min of illumination. But after only 3 min of illumination, the active centers produced near the surface of the coating were able to diffuse post-illumination, as shown in Fig. 7A and B, for 2 wt% and 3 wt% CB-35 loadings, respectively. Because the active centers have only half the thickness to diffuse within, the concentration profile becomes uniform within half the time (5 min post-illumination) compared with the 80 μm coatings in Fig. 6 (10 min post-illumination).

In industrial coatings applications, the cure time required to reach macroscopic property development ($t_{mpd}$) is especially important since it determines when coated substrate may undergo additional process steps that involve contact with the surface. At this time, the exposed surface of the coating must be tack-free, and the cure on the bottom of the coating, where it interfaces with the substrate, must be sufficient to ensure effective adhesion. For systems polymerized cationically, the time required to achieve cure at the bottom determines the $t_{mpd}$, since there is no oxygen inhibition at the exposed surface and the light intensity is the lowest at the bottom of the sample. For this reason, a conservative criterion of a 35% epoxide conversion at the bottom interface was established to predict the $t_{mpd}$. The $t_{mpd}$ was estimated by obtaining the active center concentration profiles at the bottom interface using Equation (8) (for the illumination period) and 9 (for the shadow cure period) and entering these profiles into the integrated form of the polymerization rate equation for cationic polymerization

$$\int_0^{t_{mpd}} C_{AC}\mathrm{d}t = -k_p \ln\left(\frac{m_f}{m_i}\right) \tag{11}$$

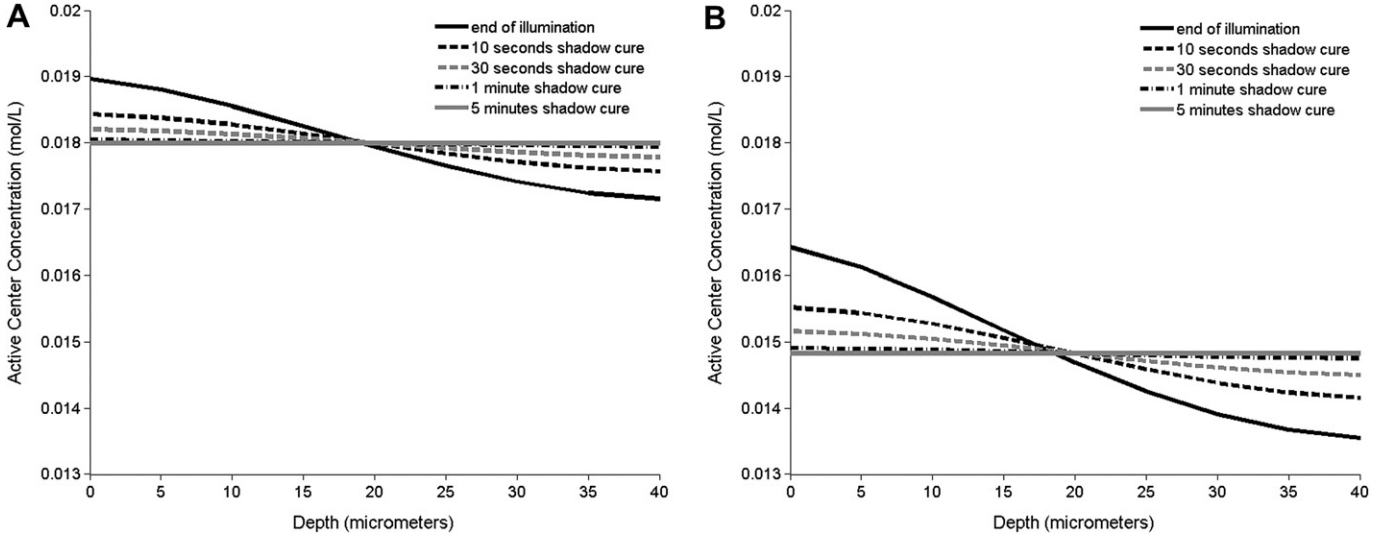


**Fig. 7.** Active center concentration profiles diffusing post-illumination in pigmented coating (40 μm thick). A) 2 wt% CB-35, B) 3 wt% CB-35. Monomer: EEC, Initiator: 1 wt% IPB, Exposure time: 3 min.

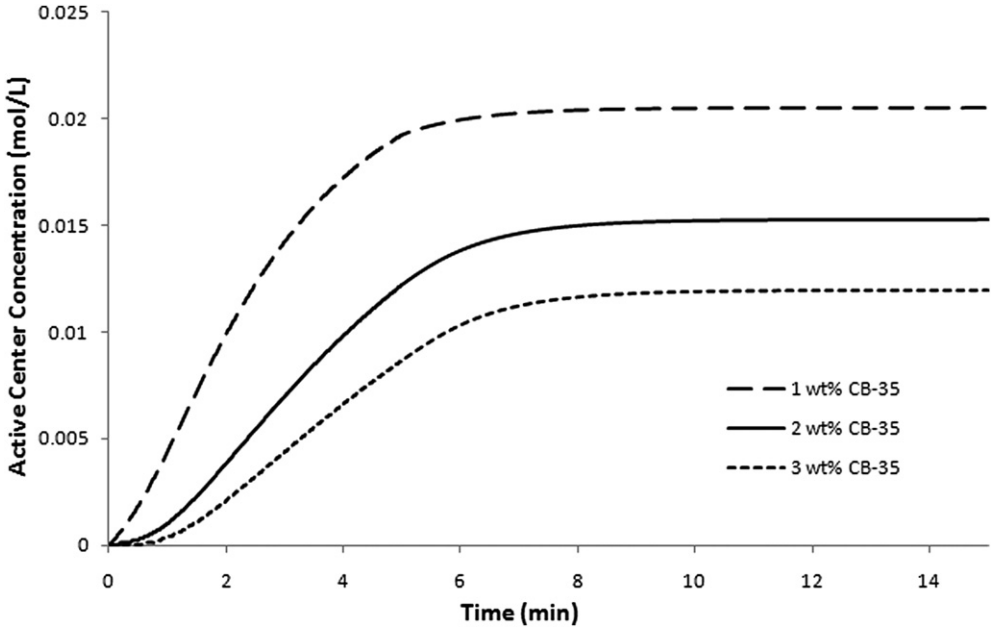


**Fig. 8.** Active center concentrations vs. time for various CB loadings at bottom interface of 80 μm thick coating. Monomer: EEC, Initiator: 1 wt% IPB, Pigment: 1–3 wt% CB-35, Exposure Time: 5 min.

where $t_{mpd}$ is the cure time required to reach macroscopic property development, $m_f/m_i$ is the ratio of final monomer concentration to initial monomer concentration, and $k_p$ is the effective propagation rate constant. As noted in the experimental section, $k_p$ was estimated using Raman spectroscopy. Experimental conversion data were combined with model predicted active center concentration data corresponding to the Raman experiment, using Equation (11), to determine a value of the effective rate constant $k_p$ of 0.1 L/mol-sec for EEC conversions below 35% (in this range of conversion, the effective propagation rate constant can be expected to remain constant, independent of conversion). This value is consistent with literature reported $k_p$ values for ring-opening polymerizations [20].

Fig. 8 contains plots of the active center concentration at the bottom interface as a function of time for 80 μm EEC coatings containing three different CB-35 loadings. In this figure, the system is illuminated for the first 5 min (active center concentration given by Equation (8)), while the final 10 min correspond to shadow cure (the active center concentration is determined by solving Equations (9) and (10)). The figure illustrates that the active center concentration reaches a plateau when the concentration becomes uniform throughout the thickness of the coating. Increasing the carbon black concentration leads to a reduced active center concentration at the bottom interface at any given time, including the plateau value when the active center concentration is uniform throughout the depth. As explained previously, this trend arises from the

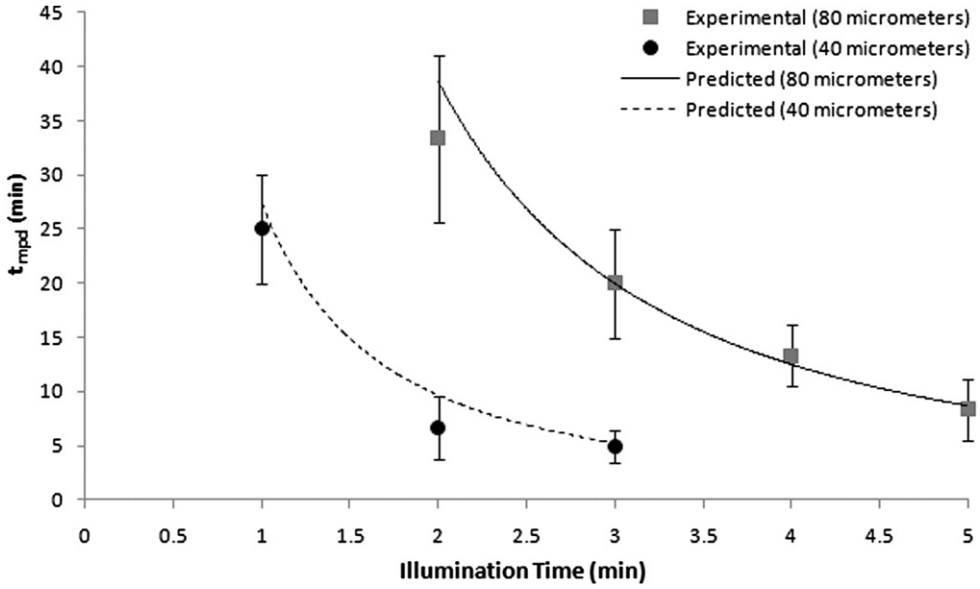


**Fig. 9.** Comparison of predicted with experimental cure times ($t_{mpd}$) at bottom interface of 40 μm and 80 μm thick coatings for varying illumination times. Monomer: EEC, Initiator: 1 wt% IPB, Pigment: 2 wt% CB-35.

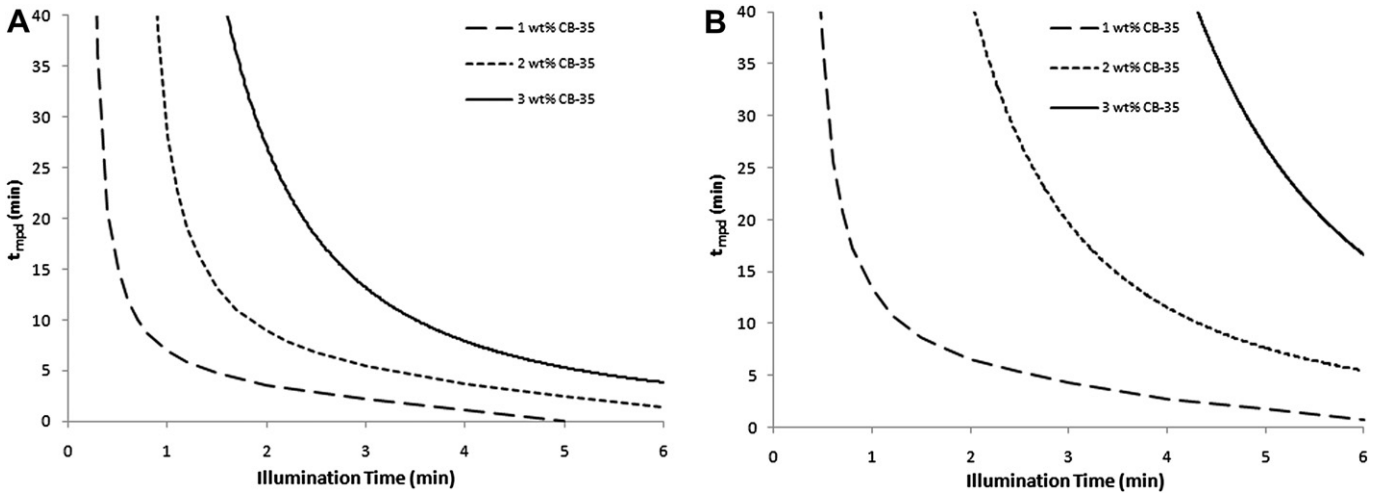


**Fig. 10.** Predicted cure times ($t_{mpd}$) at bottom interface of coatings pigmented with 1–3 wt% CB-35. A) 40 μm thickness, B) 80 μm thickness. Monomer: EEC, Initiator: 1 wt% IPB.

competitive absorption by the carbon black which reduces the total number of active centers created during illumination.

The data shown in Fig. 8 were integrated numerically to estimate the post-illumination cure time ($t_{mpd}$) by applying Equation (11), using the independently measured propagation rate constant described in the experimental section. However, Equation (11) is only valid if the carbon black neither catalyzes nor inhibits the reaction. Depending upon the method of preparation and surface treatment, the surface electronegativity of the carbon black can vary from strongly acidic to strongly basic. Based upon a standard test for characterizing the acidity or basicity of pigments such as carbon black, the CB-35 used in this study was reported to be basic (a pH of 9 from the ISO 787-9 test method was reported by the manufacturer [35]). For cationic photopolymerizations of coatings containing carbon black, a basic carbon black is preferable to ensure that the system has a desirable shelf-life. Formulations used in these experiments were stable over several months. However, due to this basicity, the CB-35 carbon black acts as an inhibitor to the cationic photoinitiator in addition to absorbing the initiating light. Therefore, the active center concentration used in Equation (11) was taken to be the theoretical concentration shown in Fig. 8 minus an inhibited active center concentration which is proportional to the carbon black loading. The value of the inhibited concentration was found to be 0.003 mol/L for each 1 wt% loading of carbon black.

Fig. 9 shows a comparison between the experimentally determined $t_{mpd}$ values and the theoretical values calculated using the procedure described above. In this figure, each data point corresponds to at least three independent experiments with the standard deviation indicated by the error bars. Recall that the $t_{mpd}$ corresponds to the time after the illumination has ceased during which the long-lived active centers continue to react and diffuse into the thickness of the coating. Fig. 9 illustrates that the predicted shape of the relationship between the post-illumination time required for macroscopic property development and the illumination time is in agreement with the experimental results. In addition, the data illustrate some interesting effects of illumination time and coating thickness. The illumination time is an important process variable since it determines the number of active centers produced, and therefore available for diffusion and cure. For this reason, the $t_{mpd}$ decreases with increasing illumination time, especially at short illumination times. As the coating thickness is increased, the required cure time increases significantly at a given illumination time.

The time for macroscopic property development is of significant practical importance since it corresponds to the earliest time in which the polymerized ink or coating can be subjected to further processing steps without risk of damaging the surface or losing adhesion to the substrate. Using the analytical approach described above, the effects of the illumination time and the carbon black loading on the post-illumination $t_{mpd}$ were investigated more thoroughly. Fig. 10 contains plots of the $t_{mpd}$ as a function of the illumination time for three different CB-35 loadings (1, 2, and 3 wt.%) and two different thicknesses (40 and 80 μm in Fig. 10A and B respectively). Recall that active centers are produced (and polymerization occurs) during the illumination time, and that the long-lived active centers continue to propagate after the illumination has ceased. The post-illumination $t_{mpd}$ will have a value of zero if the system cures during the illumination time (for example, the 1 wt% CB-35, 40 μm, 5 min illumination time case). For this reason, all of the plots will approach a value of zero as the illumination time is increased. If the illumination time is too short to produce enough active centers, the post-illumination $t_{mpd}$ will go to infinity. The threshold illumination time required to cure the coating increases with increasing CB-35 loading due to the inhibitory effect of the basic carbon black. Comparison between Fig. 10A and B shows that the thicker coatings require longer illumination times for a given post-illumination $t_{mpd}$.

## 4. Conclusions

In this contribution, the ability of long-lived cationic active centers to effectively cure coatings containing carbon black has been investigated. The slightly basic, monodisperse carbon black nanoparticle with a mean hydrodynamic radius of 29.2 nm used in these studies was found to act as a mild inhibitor of the cationic photopolymerization. The light intensity gradient and photoinitiator concentration gradient for polychromatic illumination were determined for the systems containing carbon black. The strong absorption by the carbon black resulted in sharp light intensity gradients. Consequently, the photoinitiator diffusion during the illumination period was found to have a marked effect on the resulting active center concentration profiles. Analysis of the active center reactive diffusion during the post-illumination period revealed that migration of the active centers leads to cure beyond the illuminated depth. The propagation rate equation coupled with the active center concentration profiles yielded theoretical cure times for the carbon black nanocomposite coatings. The coating

thickness and carbon black loading were found to be important variables in the time required for macroscopic property development. The long lifetimes and mobility of cationic active centers result in effective photopolymerization coatings containing carbon black, and this comprehensive approach could be applied to other opaque nanocomposite systems.

## Acknowledgements

The authors would like to thank Degussa Engineered Carbons, LP for generously donating the carbon black used in this study.

## References

[1] Wicks ZW, Jones FN, Pappas SP. Organic coatings: science and technology. New York: John Wiley & Sons, Inc.; 1994.
[2] Wetzel B, Haupert F, Zhang MQ. Composites Science and Technology 2003;63 (14):2055–67.
[3] Ng CB, Schadler LS, Siegel RW. Nanostructured Materials 1999;12(1–4):507–10.
[4] Liu Y-L, Hsu C-Y, Wei W-L, Jeng R-J. Polymer 2003;44(18):5159–67.
[5] Hartwig A, Sebald M, Kleemeier M. Polymer 2005;46(7):2029–39.
[6] Kortaberria G, Arruti P, Jimeno A, Mondragon I, Sangermano M. Journal of Applied Polymer Science 2008;109(5):3224–9.
[7] Sangermano M, Lak N, Malucelli G, Samakande A, Sanderson RD. Progress in Organic Coatings 2008;61(1):89–94.
[8] Crivello JV, Mao Z. Chemistry of Materials 1997;9(7):1562–9.
[9] Chemtob A, Croutxé-Barghorn C, Soppera O, Rigolet S. Macromolecular Chemistry and Physics 2009;210(13–14):1127–37.
[10] Sangermano M, Messori M, Galleco MM, Rizza G, Voit B. Polymer 2009;50 (24):5647–52.
[11] Sangermano M, Voit B, Sordo F, Eichhorn KJ, Rizza G. Polymer 2008;49 (8):2018–22.
[12] Decker C, Moussa K. Journal of Polymer Science Part A: Polymer Chemistry 1990;28(12):3429–43.
[13] Sipani V, Scranton AB. Journal of Photochemistry and Photobiology A-Chemistry 2003;159(2):189–95.
[14] Sipani V, Scranton AB. Journal of Polymer Science Part A: Polymer Chemistry 2003;41(13):2064–72.
[15] Ficek BA, Thiesen AM, Scranton AB. European Polymer Journal 2008;44 (1):98–105.
[16] Kenning NS, Ficek BA, Hoppe CC, Scranton AB. Polymer International 2008;57 (10):1134–40.
[17] Kenning NS, Kriks D, El-Maazawi M, Scranton AB. Polymer International 2006;55(9):994–1006.
[18] Cai Y, Jessop JLP. Polymer 2006;47:6560–6.
[19] Nelson EW, Scranton AB. Journal of Polymer Science Part A: Polymer Chemistry 1996;34(3):403–11.
[20] Odian G. Principles of polymerization. New York: John Wiley & Sons; 1991.
[21] Terrones G, Pearlstein AJ. Macromolecules 2001;34(10):3195–204.
[22] Ivanov V, Decker C. Polymer International 2001;50(1):113–8.
[23] Asmussen S, Arenas G, Cook WD, Vallo C. European Polymer Journal 2009;45 (2):515–22.
[24] Baikerikar KK, Scranton AB. Polymer 2001;42(2):431–41.
[25] Baikerikar KK, Scranton AB. Journal of Applied Polymer Science 2001;81: 3449–61.
[26] Narayanan V, Scranton AB. Trends in Polymer Science 1997;5:415–9.
[27] Coons LS, Rangarajan B, Godshall D, Scranton AB. Photopolymerization, ACS symposium series 673 1997:203–218.
[28] Miller GA, Gou L, Narayanan V, Scranton AB. Journal of Polymer Science - Polymer Chemistry Edition 2002;40(6):793–808.
[29] Azan V, Lecamp L, Lebaudy P, Bunel C. Progress in Organic Coatings 2007;58 (1):70–5.
[30] Jahn R, Jung T. Progress in Organic Coatings 2001;43(1–3):50–5.
[31] Tesfamichael T, Hoel A, Wackelgard E, Niklasson GA, Gunde MK, Orel ZC. Solar Energy 2000;69(1–6):35–43.
[32] Cussler EL. Diffusion: mass transfer in fluid systems. New York: Cambridge University Press; 1984.
[33] Anseth KS, Wang CM, Bowman CN. Macromolecules 1994;27(3):650–5.
[34] Nelson EW, Jacobs JL, Scranton AB, Anseth KS, Bowman CN. Polymer 1995;36(24).
[35] Tauber G, Hasenzahl S, Johnson RE. Evonik Industries. NIPex Pigment blacks for toner: technical information No. 1025, 2008.